



Science Arts & Métiers (SAM)

is an open access repository that collects the work of Arts et Métiers Institute of Technology researchers and makes it freely available over the web where possible.

This is an author-deposited version published in: <https://sam.ensam.eu>
Handle ID: <http://hdl.handle.net/10985/18644>

To cite this version :

Jean GILLIBERT, Mathias BRIEU, Julie DIANI - Anisotropy of direction-based constitutive models for rubber-like materials - International Journal of Solids and Structures - Vol. 47, n°5, p.640-646 - 2010

Any correspondence concerning this service should be sent to the repository

Administrator : scienceouverte@ensam.eu



Anisotropy of direction-based constitutive models for rubber-like materials

Jean Gillibert^a, Mathias Brieu^{a,*}, Julie Diani^b

^a LML, Ecole Centrale de Lille, bd Paul Langevin, 59650 Villeneuve d'Ascq, France

^b CNRS, Arts et Metiers ParisTech, LIM, 151 bd de l'Hopital 75013 Paris, France

A B S T R A C T

A study of direction-based models for the representation of isotropic and anisotropic hyperelastic behaviour of rubber-like materials is proposed. The interest in such models is sustained by their ability to account for the Mullins effect induced anisotropy. For such a purpose, the directional models should be initially isotropic and representative of the hyperelastic behaviour of rubber-like materials. Various models were defined according to different sets of directions. Models were tested in terms of their initial anisotropy and their ability to reproduce the classic full-network hyperelastic behaviour. Various models were proved to perform very well.

Keywords:

Rubbers
Non-linear elasticity
Large deformation
Anisotropy

1. Introduction

Rubber-like materials are made of very long macromolecular chains crosslinked into three-dimension polymer networks. The length of the chains enables the high deformability and the network structure provides the material with elasticity.

The early theory accounting for rubber elasticity is based on the statistical treatment of the network defined by the assembly of chains consisting of bonds of random directions in space. It is grounded on a thermodynamics analysis showing that large deformations in rubber-like materials result from a change of entropy. The total entropy change of a bulk material is obtained by summation of the change of entropy of each chain. Explicit macromolecular models were first introduced for specific chain configurations in the 40s. (An extended account of the macromolecular theory of rubber elasticity may be found in Treloar (1975).)

Usually, the spatial distribution of chain orientations in a virgin bulk material draws a sphere, which explains the initial isotropy of rubbers. Treloar (1954) accounted for such a representation in the full-network model and Treloar and Riding (1979) computed the integration over the surface of a sphere of the elementary change of entropy. Although, this model was shown later to drive to constitutive relations depending on simple elliptic integrals (Perrin, 2000), it proved to be difficult to handle in finite element analysis. In an effort of simplification, Wu and van der Giessen (1993) successfully approximated the full integration model by combining the 3-chain (Wang and Guth, 1952) and the 8-chain (Arruda and Boyce, 1993) models. In these last models, the actual network is

represented by a finite number (3 and 8, respectively) of directions, which follows the principal directions of the gradient deformation tensor in order to satisfy to the isotropy of the material. This drives to simple analytical stress–strain relations. The main drawback of such models stands in their inability to evolve from isotropic models to anisotropic ones. Indeed, rubber-like materials exhibit induced anisotropy due to mechanical loadings. More precisely, during the first loading, the virgin material undergoes a stress-softening known as the Mullins effect (reviewed in Mullins (1969) and Diani et al. (2009)), which is much more important in the direction of stretch than in the other ones (Mullins, 1948, 1949; Laraba-Abbes and Ienny, 2003; Hanson et al., 2005; Diani et al., 2006). Anisotropy may also arise from the manufacturing process (Robisson, 2000; Diani et al., 2004) or from a structural effect like in rubber composites reinforced by fibers (Nechwatal et al., 2008).

In order to fit an anisotropy resulting from the Mullins effect, the manufacturing process or the material structure, material direction-based constitutive models were recently introduced (Diani et al., 2004, 2006; Göktepe and Miehe, 2005). These models are very much alike the macromolecular ones except for the choice of directions, which do not follow the principal directions of the gradient deformation but are materials. The set of directions is chosen according to the initial isotropy or anisotropy of the material. Isotropic virgin rubbers may transform into anisotropic materials, as the result of material softening in specific directions according to the loading history (Göktepe and Miehe, 2005; Diani et al., 2006). Therefore, in a material direction-based model, the number of directions must be sufficient to provide with initial isotropy and must be limited to favour finite element computations.

In a context of infinitesimal strains, Bažant and Oh (1986) introduced various sets of directions and evaluated the anisotropy of

* Corresponding author. Tel.: +33 320335375; fax: +33 320335499.
E-mail address: mathias.brieu@ec-lille.fr (M. Brieu).

the non-linear elastic modelled materials, by comparing the stress responses to a uniaxial stretch according to the direction of stretching. Estimating the anisotropy of a mechanical behaviour law is still of actuality in linear elasticity (Moakher and Norris, 2006). In order to assess the anisotropy of the non-linear hyper-elastic models for various types of loadings, we defined anisotropy rates depending on the loading intensity and the loading type, which are characterized by two invariants of the logarithmic strain tensor. The anisotropy rates were computed and plotted for various discrete representations of the affine full network, not limited to the directions reported by Bažant and Oh (1986). As expected, the model anisotropies depend on the number and orientations of the directions. The low-anisotropy models compared favourably to the full-network model, diverging for loadings of extreme intensity only.

2. Material direction-based constitutive models

2.1. Constitutive equations

Rubber-elastic materials may be characterized by a strain-energy function \mathcal{W} depending on the deformation gradient \underline{F} . In the case of directional models, the strain-energy function is defined by:

$$\mathcal{W}(\underline{F}) = \nu \sum_{i=1}^m \omega^i w(v^i) \quad (1)$$

where $v^i = \sqrt{(\underline{F}\underline{u}^i)^T \cdot (\underline{F}\underline{u}^i)}$ is the stretch applied in the direction defined by the unit vector \underline{u}^i , the parameter ω^i characterizes the weight matching direction \underline{u}^i and $\sum_i \omega^i = 1$, w is the elementary strain energy, and m is the number of directions. In the case of ideal isotropy, every direction is equally balanced, their number m tends toward infinity. In such a case, the strain-energy density (1) transforms into:

$$\mathcal{W}(\underline{F}) = \frac{\nu}{4\pi} \int_{\theta=0}^{\pi} \int_{\phi=0}^{2\pi} w(v) ds \quad \text{with } ds = \sin \theta d\theta d\phi \quad (2)$$

which corresponds to the full-network model strain-energy density (Treloar and Riding, 1979). From a macromolecular point of view, ν characterizes the density of chains supporting the stresses, from a mechanical point of view, ν is proportional to the material shear modulus.

The elementary strain energy density, w , may be chosen of various forms. In this study, we adopt to use the elementary strain energy provided by the macromolecular models. In the latter ones, w arises from a statistical calculation of the macromolecular entropy of a single molecular chain. It writes as:

$$w(v) = k_B T N \left(\beta(v) \frac{v}{\sqrt{N}} + \ln \left(\frac{\beta(v)}{\sinh \beta(v)} \right) \right) \quad \text{with } \beta(v) = L^{-1} \left(\frac{v}{\sqrt{N}} \right)$$

which leads to $\frac{dw}{dv} = k_B T \sqrt{N} L^{-1} \left(\frac{v}{\sqrt{N}} \right)$ (3)

where k_B is Boltzmann's constant, T the absolute temperature, and v cannot exceed \sqrt{N} , which designates the limit of extension of the chains. The function L^{-1} is the inverse of the Langevin's function $L(x) = \coth(x) - \frac{1}{x}$ and was introduced by Kuhn and Gr \ddot{u} n (1942) for an account of large deformations. For analytical and numerical conveniences, it is usually approximated by a Pad \acute{e} approximant or a polynomial function introduced by Cohen (1991) and Kuhn and Kuhn (1946), respectively:

$$L_{\text{Pad}\acute{e}}^{-1}(x) = x \frac{3 - x^2}{1 - x^2} \quad (4)$$

$$L_{\text{Poly}}^{-1}(x) = 3x + \frac{9}{5}x^3 + \frac{297}{175}x^5 + \frac{1539}{875}x^7 + \frac{126117}{67375}x^9 + \dots$$

The error involved in the use of an approximation is shown in Fig. 1. Both approximants provide with a very good approximation of the inverse Langevin function as long as $x \leq 0.8$. For $x \in]0.8, 1[$, which corresponds to deformations close to the limit of extension, the Pad \acute{e} approximant is to be preferred.

Considering an incompressible isotropic rubber characterized by (1), the Cauchy stress tensor writes as:

$$\underline{\sigma} = \frac{\partial \mathcal{W}}{\partial \underline{F}} \underline{F}^T - p \underline{1} \quad (5)$$

where p is a Lagrange Multiplier resulting from the incompressibility assumption. The latter assumption is favoured by infinitesimal volume changes in rubbers when submitted to loading conditions such as uniaxial tension, biaxial tension, pure shear, etc.

Let us note that when considering the special cases for which the deformation gradient \underline{F} is symmetric, one may write the principal Cauchy stresses σ_i as,

$$\sigma_k = \tilde{\sigma}_k - p \quad \forall k = \{1, 2, 3\} \quad (6)$$

where $\tilde{\sigma}_k$ writes as,

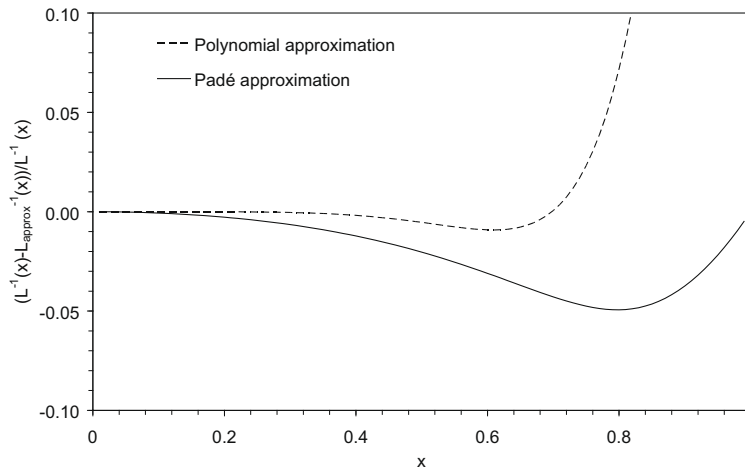


Fig. 1. Normalized difference between the inverse Langevin function L^{-1} and its approximants (4).

$$\tilde{\sigma}_k = v \sum_{i=1}^m \omega^i k_B T \sqrt{NL}^{-1} \left(\frac{v^i}{\sqrt{N}} \right) \frac{\partial v^i}{\partial \lambda_k} \lambda_k \quad (7)$$

when the elementary strain energy density w is defined by (3) and when the three principal stretches, defining the eigenvalues of \underline{F} , are noted $\lambda_1 \geq \lambda_2 \geq \lambda_3 \geq 0$ ($\lambda_1 \lambda_2 \lambda_3 = 1$). Note that when \underline{u}^i is defined by (u_1^i, u_2^i, u_3^i) in \mathcal{B}_F the principal basis of \underline{F} , $\frac{\partial v^i}{\partial \lambda_k} = \frac{\lambda_k(u_k^i)}{v^i}$.

One notes that Eqs. (6) and (7) depend strongly on the number and the orientations of the model directions. In the following section, we introduce various sets of directions, which could apply.

2.2. Sets of directions

Bažant and Oh (1986) calculated and reported several sets of directions appropriate for efficient numerical integrations on the surface of a sphere. Each set of directions is defined by the vectors connecting the center to the vertices of a specific polyhedron (Fig. 2). New polyhedrons are defined by adding vertices at the centers of the edges or faces of existing polyhedrons. In order to achieve accurate integrations of polynomial functions, directions are balanced by specific weights, ω^i . The coordinates of the vectors and the values of their weights are listed in Bažant and Oh (1986). We exploited five sets of directions of 32, 42, 66, 74 and 122 directions, respectively. Bažant and Oh (1986) defined the degree of a set of directions by the maximum degree of the polynoms exactly integrated on the surface of the sphere by the discrete system. The 32 and 42-point sets are 9th-degree, the 66-point is a 11th-degree set, while the 74-point and the 122-point are 13th-degree sets, but the 122-point is not fully symmetric, which will discuss later.

A second family of sets of directions was built using a simple iterative process. From a first set of directions, we start a larger set of directions consisting of the directions of the previous set added of new directions defined by the vectorial sum of three existing directions and their orthogonal symmetries (Fig. 2). Starting with the orthogonal basis $(\underline{e}^1, \underline{e}^2, \underline{e}^3)$, one builds a first set of six directions, $(\underline{u}^1 = \underline{e}^1, \underline{u}^2 = \underline{e}^2, \underline{u}^3 = \underline{e}^3, \underline{u}^4 = -\underline{e}^1, \underline{u}^5 = -\underline{e}^2, \underline{u}^6 = -\underline{e}^3)$. Then at the first step of the iterative process, 14 directions are defined using: $\underline{u}^1, \underline{u}^2, \underline{u}^3$ and their symmetries $-\underline{u}^1, -\underline{u}^2, -\underline{u}^3$ added of $\underline{u}^7 = \frac{\underline{u}^1 + \underline{u}^2 + \underline{u}^3}{\sqrt{3}}$ and its seven symmetries: $\frac{-\underline{u}^1 - \underline{u}^2 - \underline{u}^3}{\sqrt{3}}, \frac{-\underline{u}^1 + \underline{u}^2 + \underline{u}^3}{\sqrt{3}}, \frac{-\underline{u}^1 - \underline{u}^2 + \underline{u}^3}{\sqrt{3}}, \frac{-\underline{u}^1 + \underline{u}^2 - \underline{u}^3}{\sqrt{3}}, \frac{-\underline{u}^1 - \underline{u}^2 - \underline{u}^3}{\sqrt{3}}, \frac{-\underline{u}^1 + \underline{u}^2 - \underline{u}^3}{\sqrt{3}},$ and $\frac{-\underline{u}^1 + \underline{u}^2 + \underline{u}^3}{\sqrt{3}}$. At the second step, 38 directions are built based on $(\underline{u}^1, \underline{u}^2, \underline{u}^3, \underline{u}^7)$ (see Table 1). Following this process, we built sets of 6, 14, 38 and 110 directions. For each set of directions, we note that if \underline{u}^i is one of the set direction that $-\underline{u}^i$ is also. Like in the case of the direction sets based on polyhedron geometries, weights ω^i may be calculated according to

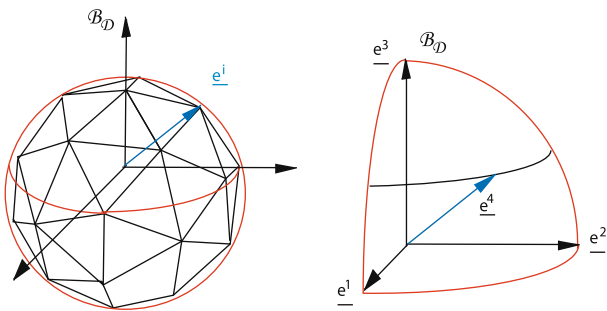


Fig. 2. Construction of material directions. Left: sets of directions are defined by the vertices of polyhedrons, which are built one from the other by adding vertices at the center of the faces or edges (see Bažant and Oh (1986) for more details). Right: sets of material directions are built using an iterative scheme, directions of a new set being defined by the directions of the previous set added of the vectorial sums of three directions existing at the previous iteration.

Table 1
Direction and weights of the 2×19 -direction set.

	$(\underline{u}^i)_1$	$(\underline{u}^i)_2$	$(\underline{u}^i)_3$	ω_i
1	1.0	0.0	0.0	0.0584319
2	0.0	1.0	0.0	
3	0.0	0.0	1.0	
4	0.577350269	0.577350269	0.577350269	0.0436761
5	-0.577350269	0.577350269	0.577350269	
6	-0.577350269	-0.577350269	0.577350269	
7	0.577350269	-0.577350269	0.577350269	
8	0.684550319	0.684550319	0.250562807	0.0125000
9	0.250562807	0.684550319	0.684550319	
10	0.684550319	0.250562807	0.684550319	
11	-0.684550319	0.684550319	0.250562807	
12	-0.250562807	0.684550319	0.684550319	
13	-0.684550319	0.250562807	0.684550319	
14	-0.684550319	-0.684550319	0.250562807	
15	-0.250562807	-0.684550319	0.684550319	
16	-0.684550319	-0.250562807	0.684550319	
17	0.684550319	-0.684550319	0.250562807	
18	0.250562807	-0.684550319	0.684550319	
19	0.684550319	-0.250562807	0.684550319	

procedure reported in Bažant and Oh (1986) to obtain the highest degree for each sets. The direction coordinates, \underline{u}^i ($\underline{u}_1^i, \underline{u}_2^i, \underline{u}_3^i$), and weights ω_i , are reported in Tables 1 and 2 for the 7th-degree 38-direction and the 9th-degree 110 direction sets, respectively.

Table 2
Direction and weights of the 2×55 -direction set.

	$(\underline{u}^i)_1$	$(\underline{u}^i)_2$	$(\underline{u}^i)_3$	ω_i
1–3	Coordinates defined Table 1			0.03735430
4–7	Coordinates defined Table 1			0.00269572
8–19	Coordinates defined Table 1			0.01250000
20	0.831826946	0.464071197	0.304469794	0.00630984
21	0.703227911	0.703227911	0.104599285	
22	0.464071197	0.831826946	0.304469794	
23	0.304469794	0.831826946	0.464071197	
24	0.104599285	0.703227911	0.703227911	
25	0.304469794	0.464071197	0.831826946	
26	0.464071197	0.304469794	0.831826946	
27	0.703227911	0.104599285	0.703227911	
28	0.831826946	0.304469794	0.464071197	
29	-0.831826946	0.464071197	0.304469794	
30	-0.703227911	0.703227911	0.104599285	
31	-0.464071197	0.831826946	0.304469794	
32	-0.304469794	0.831826946	0.464071197	
33	-0.104599285	0.703227911	0.703227911	
34	-0.304469794	0.464071197	0.831826946	
35	-0.464071197	0.304469794	0.831826946	
36	-0.703227911	0.104599285	0.703227911	
37	-0.831826946	0.304469794	0.464071197	
38	-0.831826946	-0.464071197	0.304469794	
39	-0.703227911	-0.703227911	0.104599285	
40	-0.464071197	-0.831826946	0.304469794	
41	-0.304469794	-0.831826946	0.464071197	
42	-0.104599285	-0.703227911	0.703227911	
43	-0.304469794	-0.464071197	0.831826946	
44	-0.464071197	-0.304469794	0.831826946	
45	-0.703227911	-0.104599285	0.703227911	
46	-0.831826946	-0.304469794	0.464071197	
47	0.831826946	-0.464071197	0.304469794	
48	0.703227911	-0.703227911	0.104599285	
49	0.464071197	-0.831826946	0.304469794	
50	0.304469794	-0.831826946	0.464071197	
51	0.104599285	-0.703227911	0.703227911	
52	0.304469794	-0.464071197	0.831826946	
53	0.464071197	-0.304469794	0.831826946	
54	0.703227911	-0.104599285	0.703227911	
55	0.831826946	-0.304469794	0.464071197	

In order to provide the reader with a visual sense of the distribution of the directions, each direction set has been represented using a Lambert azimuthal projection in Fig. 3. In this Figure, we observe that the 66-direction and the 122-direction sets reported in Bažant and Oh (1986) seems to offer a relatively uniform distribution of orientations.

2.3. Material anisotropy

In order to assess the initial isotropy of a material direction-based model, one has to define a measure of anisotropy. It is simple to verify that some models are anisotropic but it is delicate to compare them in terms of their anisotropy. For example, Bažant and Oh (1986) evaluated the anisotropy of each of their models by calculating the difference between the uniaxial stresses resulting from a uniaxial tension according to various directions. In order to extend this anisotropy characterization to all kind of loading conditions, we propose to characterize the loading conditions by $h_{eq} = \sqrt{(\ln \lambda_1)^2 + (\ln \lambda_2)^2 + (\ln \lambda_3)^2}$ and $\rho = \frac{3 \ln \lambda_2}{\ln \lambda_1 - \ln \lambda_3}$, the invariants of the logarithmic tensor $\underline{H} = \frac{1}{2} \ln \underline{F} \underline{F}^T$, instead of $\lambda_1, \lambda_2, \lambda_3$. Indeed, h_{eq} and ρ designate the intensity of deformation and the type of deformation, respectively. By definition $h_{eq} \geq 0$ and ρ varies from -1 , corresponding to a uniaxial compression or equi-biaxial tension, to $+1$, characterizing the uniaxial tension. Then, the parameter of anisotropy may be calculated according to the type of loadings for an identical intensity of deformation. For this purpose, we introduce \mathcal{A} , a matrix of rotation defined by three angles (θ, ϕ, ψ) , and which defines the rotation transforming the basis of the material direction basis \mathcal{B}_D into the basis defined by the eigenvectors of \underline{C} . Then, we define the anisotropy parameter \mathcal{A} by,

$$\mathcal{A} = \frac{\max_{(\theta, \phi, \psi)} X(h_{eq}, \rho) - \min_{(\theta, \phi, \psi)} X(h_{eq}, \rho)}{\max_{(\theta, \phi, \psi)} X(h_{eq}, \rho)} \quad (8)$$

X designating a measure of the material “response” to the applied deformation. Many quantities may apply to X , we consider three of them,

- The strain–energy density:

$$X = \mathcal{W} \quad (9)$$

- The von Mises equivalent stress:

$$X = \sigma_{eq} = \sqrt{\frac{3}{2} (s_1^2 + s_2^2 + s_3^2)} \quad (10)$$

s_k being the principal stresses of the deviatoric part of the Cauchy stress tensor.

- The Tresca equivalent stress:

$$X = \max_{k,l} |\sigma_k - \sigma_l| \quad (11)$$

The degree of anisotropy, \mathcal{A} , defined accordingly to (9), can be easily estimated for any kind of loadings (symmetric and non-symmetric deformation gradient tensors). Values of X for (10) or (11) are more difficult to reach in the case of non-symmetric deformation gradient tensors than for symmetric ones. Therefore, for reasons of simplicity and as a first approach, we limited ourselves to the cases of loadings inducing symmetric deformation gradient tensors. We note that for every expression of X , \mathcal{A} is null when the material is isotropic. Anisotropy \mathcal{A} depends on the set of directions and their respective weights and on the material parameter N .

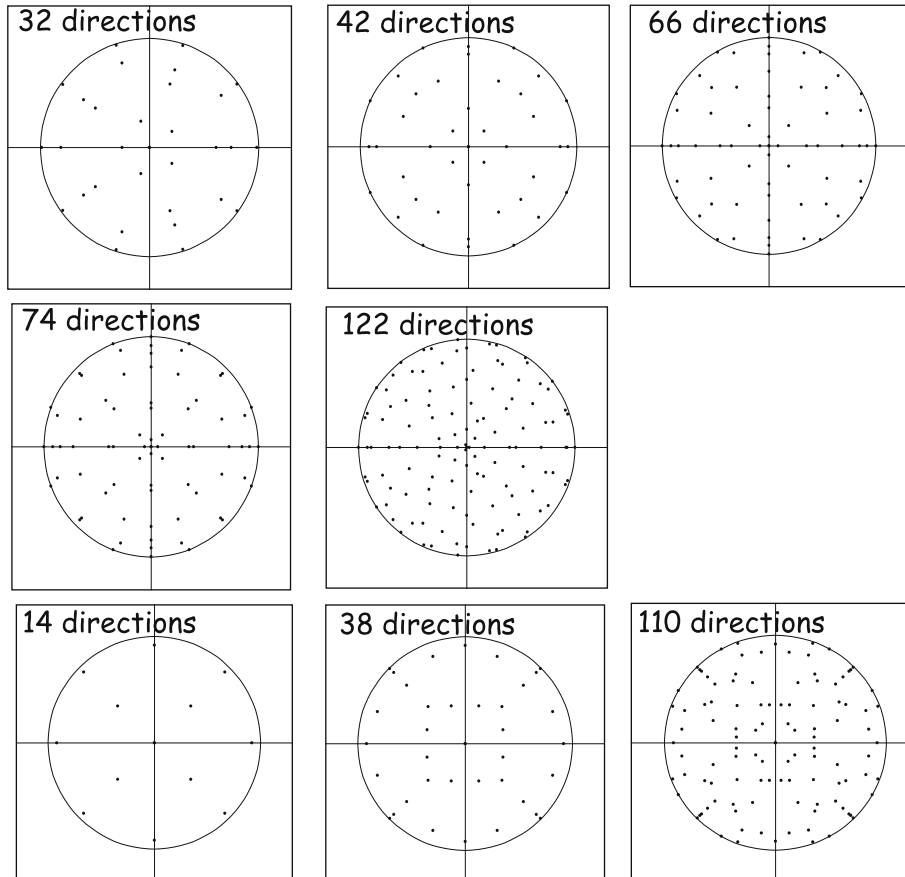


Fig. 3. Lambert azimuthal projection of the direction sets.

2.4. Approximation of the full integration

Initially isotropic rubber-like materials are made of randomly oriented macromolecular chains. For such a reason, the full-network model, (2) consisting of a full integration over a sphere, appears as a realistic representation of the contribution of each macromolecule. As mentioned earlier, directional models, based on a discrete summation over a number of chosen directions, were developed for anisotropic materials and also for initially isotropic materials evolving towards anisotropic ones. Within isotropic assumption, directional models should compare favourably to the full-network model.

Denoting v^d and N^d , and v^f and N^f , the parameters of the directional models and the full-network model, respectively, these parameters must satisfy to certain conditions in order to fit the same material behaviour. Since $\sqrt{N^d}$ represents the maximal stretch sustained by the model directions, assuming $N^f = N^d$ will guaranty the same limit of extension in the privileged directions. Considering $v^d = v^f$ will compare two materials of identical initial stiffness (same shear modulus).

In the following, models will be compared with respect to the anisotropy rates and the full-network representation.

3. Results and discussion

3.1. Anisotropy of discrete networks

In order to first evaluate the sensitivity of the anisotropy rates defined according to the parameters X in (9)–(11), we computed values of \mathcal{A} for the 6-direction model. The intensity of loading is set to one ($h_{eq} = 1$) and ρ varies in the range of $[-1,1]$ covering every loading conditions from equi-biaxial tension to uniaxial tension. Results are shown in Fig. 4 for a material with $N = 26$ (this value corresponds to the fit of classic data (Arruda and Boyce, 1993)). For the three anisotropy rates, the uniaxial tension ($\rho = 1$) appears to be the most discriminant in terms of isotropy. The energy-based anisotropy rate shows significantly lower values than the other anisotropy rates; the strain energy appears to be insufficient to track the anisotropy of the models. The anisotropy rate based on the Tresca equivalent stress shows a particular drop when ρ tends toward -1 . This particular feature was observed for the 6-direction model only and thus has to be related to the low number of directions creating a discontinuity. In the following, only values of the anisotropy rate calculated with the von Mises equivalent stress

(10) will be presented. Indeed, similar results were obtained with the Tresca equivalent stress (11) for the results we report.

In order to study the influence of the model parameters N , we set $h_{eq} = 1$ and $\rho = 1$ and computed \mathcal{A} as a function of N for the 6-direction model. Fig. 5 illustrates the change of anisotropy vs. N . A lower limit value of N equal to 10 was set in order to avoid stretches close of the limit of extension (\sqrt{N}). The model anisotropy increases with the decrease of N . Actually, a decrease of N is equivalent to an increase of the intensity of loading h_{eq} , therefore and as expected, anisotropy increases with the loading intensity. In the following, every result was obtained with $N = 10$ in order to exhibit high anisotropy.

Next, the model anisotropy was computed according to the set of directions and the type of loading ($-1 \leq \rho \leq 1$) for a loading intensity of $h_{eq} = 1$. Results provided by the direction sets built with the iterative scheme are shown in Fig. 6a, while those provided by the direction sets based on polygons are given in Fig. 6b. In Fig. 6a, one observes, as expected that the model tends toward isotropy when increasing the number of directions. Nonetheless, direction sets used by Bažant and Oh (1986) provide lower anisotropies (Fig. 6b). There are interests in choosing the 32-direction model, since it exhibits lower anisotropy and lower calculation duration than the 110-direction model. Also, we note that 66-direction model shows less anisotropy than the 74-direction model, which supports the visual impression (Fig. 3) of uniform distribution of orientations of the 66-direction model. Finally, we observe that the 122-direction model is not less anisotropic than the 66-direction model for all values of ρ . Actually, for values of ρ lower than 0.4, the 66-direction model displays less anisotropy. This is probably due to the full symmetry property of the 66-direction model, which is not shared by the 122-direction model.

With this anisotropy investigation done, we now compare the proposed directional models to the full-network.

3.2. Discrete networks vs. full-network

As mentioned earlier, the full-network is probably the most intuitive representation for isotropic rubber-like materials. Then, in order to decide of the interest of the directional models, it is not only necessary that these models can fit isotropy but also that they can reproduce the full-network behaviour. For this reason, we performed a comparison of the discrete networks with the full network assuming, as explained in Section 2.4, $N^d = N^f$ and $v^d = v^f$. The difference between the discrete models and the full-network

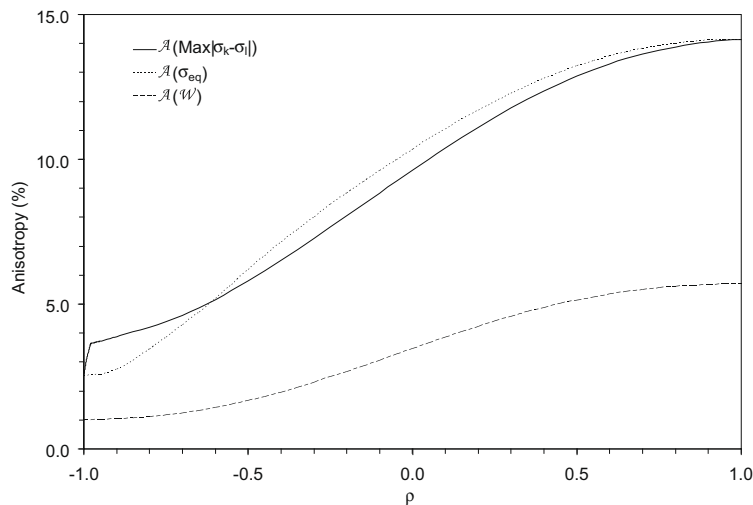


Fig. 4. Comparison of the anisotropy rates $\mathcal{A}(X)$ according to the type of loading conditions for a loading intensity $h_{eq} = 1$ and for the 6-direction model with $N = 26$.

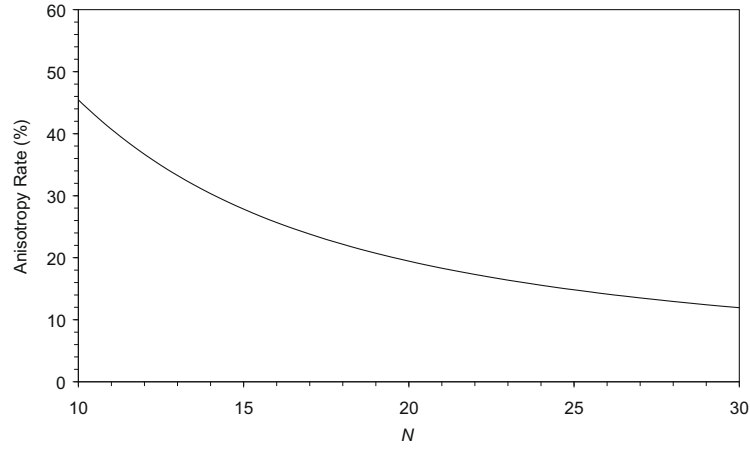


Fig. 5. Anisotropy rate of the 6-direction model in uniaxial tension vs. the model parameter of extension limit N .

model in uniaxial tension is shown in Fig. 7 in terms of the error (%) generated by a discrete integration vs. loading intensity. Fig. 7 shows the ability of directional models to replicate the full-network model for moderate to large stretches according to the model. Each directional model diverges from the full-network model when the stretching exceeds a limit. This stretch limit depends

on the direction set but appears to be higher for direction sets based on polygon geometries. In order to give a quantitative idea of the stretch limit, we report a difference between the full-network uniaxial response and the 122-direction model response of less than 1% for stretches below 306%, when the theoretical stretch cannot exceed 316% due to the value of N (10).

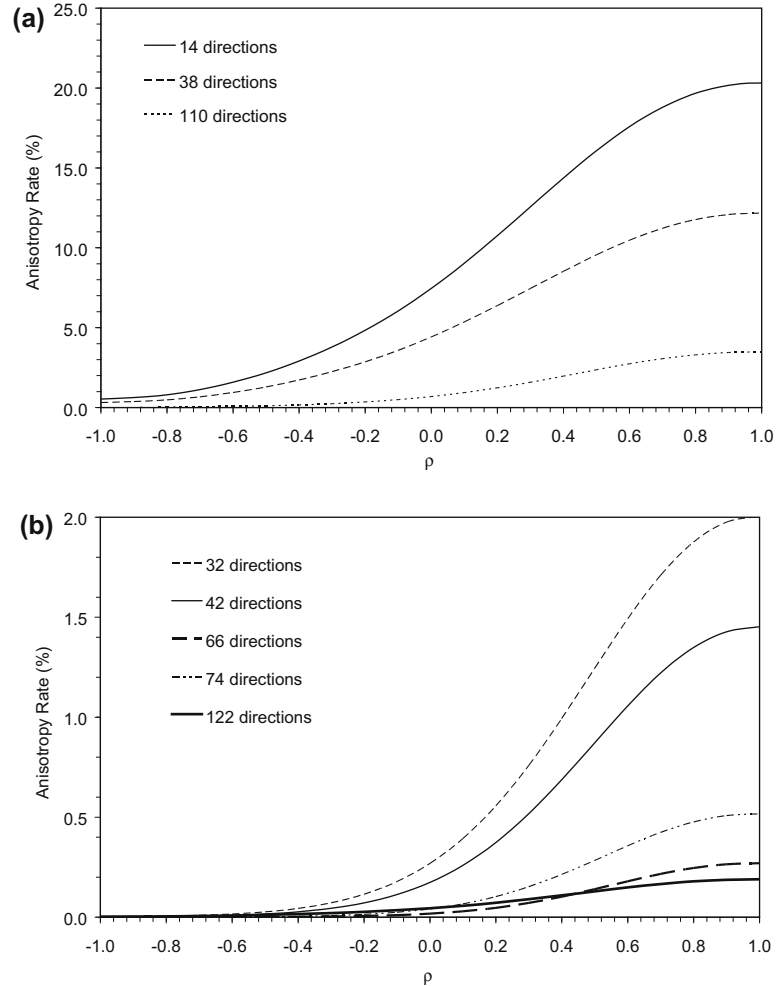


Fig. 6. Anisotropy of the directional models for an intensity loading of $h_{eq} = 1$ vs. the type of loading ($N = 10$). (a) Models based on direction sets built using an iterative scheme. (b) Models based on Bažant and Oh (1986) direction sets.

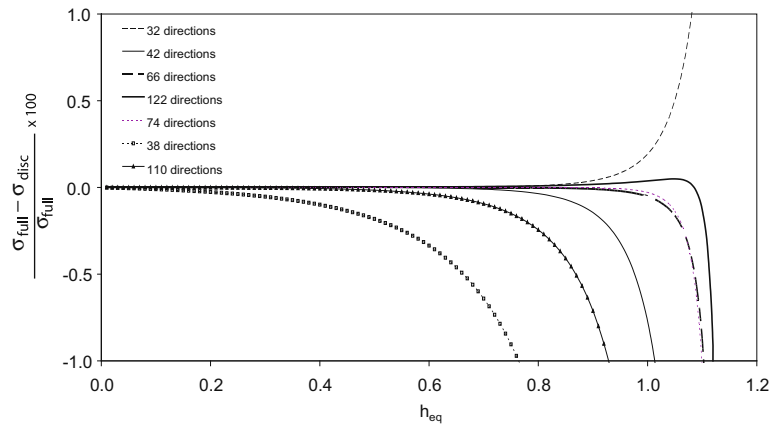


Fig. 7. Difference between the responses of discrete networks and the full-network for a uniaxial tension loading.

4. Conclusion

We investigated specific models referred as directional models, designed for the representation of the hyperelastic behaviour of isotropic and anisotropic rubber-like materials. The main interest of such models is their abilities to evolve from isotropy to anisotropy by a non-homogeneous alteration of the material stiffness according to the directions. In order to propose an efficient initially isotropic directional model, we introduced several sets of directions, and tested the models according to their anisotropies and their abilities to reproduce the classic full-network isotropic behaviour. Three parameters of anisotropy were proposed based on the strain energy density, the Mises equivalent stress and the Tresca equivalent stress, respectively. Model anisotropy was estimated according to the direction set, the type of loadings (although, only loadings with symmetric deformation gradient tensors were considered so far) and the loading intensity. The uniaxial tension loading proved to be discriminant to characterize the model anisotropy. Excellent isotropy performances were obtained for Bažant and Oh (1986) discrete model. These models were also successfully compared to the full-network model.

References

- Arruda, E., Boyce, M.C., 1993. A three-dimensional constitutive model for the large stretch behaviour of rubber elastic materials. *Journal of Mechanics and Solids* 41, 389–412.
- Bažant, Z.P., Oh, B.H., 1986. Efficient numerical integration on the surface of a sphere. *Zeitschrift für Angewandte Mathematik und Mechanik* 66 (1), 37–49.
- Cohen, A., 1991. A padé approximant to the inverse Langevin function. *Rheologica Acta* 30, 270–273.
- Diani, J., Brieu, M., Vacherand, J.M., Rezgui, A., 2004. Directional model for isotropic and anisotropic hyperelastic rubber-like materials. *Mechanics of Materials* 36, 313–321.
- Diani, J., Brieu, M., Gilormini, P., 2006. Observation and modeling of the anisotropic visco-hyperelastic behaviour of rubber-like materials. *International Journal of Solids and Structures* 43, 3044–3056.
- Diani, J., Fayolle, B., Gilormini, P., 2009. A review on the Mullins effect. *European Journal of Polymer* 45 (3), 601–612.
- Göktepe, S., Miehe, C., 2005. A micro-macro approach to rubber-like materials. Part III: the micro-sphere model of anisotropic Mullins-type damage. *Journal of Mechanics and Solids* 53 (10), 2259–2283.
- Hanson, D.E., Hawley, M., Houlton, R., Chitanvis, K., Rae, P., Orler, E.B., Wroblewski, D.A., 2005. Stress softening experiments in silica-filled polydimethylsiloxane provide insight into a mechanism for the Mullins effect. *Polymer* 46, 10989–10995.
- Kuhn, W., Gr \ddot{u} n, F., 1942. Beziehungen zwischen elastischen Konstanten und Dehnungsdoppelbrechung hochelastischer Stoffe. *Kolloid-Zeitschrift* 101, 248–271.
- Kuhn, W., Kuhn, H., 1946. Statistische und energieelastische Rückstellkraft bei stark auf Dehnung beanspruchten Fadenmolekeln. *Helvetica Chimica Acta* 29 (5), 1095–1115.
- Laraba-Abbes, F., Ienny, P., 2003. A new Taylor-made methodology for the mechanical behaviour analysis of rubber-like materials: II. Application to the hyper-elastic behaviour characterization of a carbon-black filled natural rubber vulcanizate. *Polymer* 44, 821–840.
- Moakher, M., Norris, A.N., 2006. The closest elastic tensor of arbitrary symmetry to an elasticity tensor of lower symmetry. *Journal of Elasticity* 85, 215–263.
- Mullins, L., 1948. Effect of stretching on the properties of rubber. *Journal of Rubber Research* 16, 275–282.
- Mullins, L., 1949. Permanent set in vulcanized rubber. *India Rubber World* 120, 63–66.
- Mullins, L., 1969. Softening of rubber by deformation. *Rubber Chemistry and Technology* 42, 339–362.
- Nechwatal, A., Hauspurg, C., Fiedler, D., Fidler, S., 2008. Anisotropic compression set of elastomer products by short fibers. *Technische Textilien* 51 (2), 74–76.
- Perrin, G., 2000. Analytic stress-strain relationship for isotropic network model of rubber elasticity. *Compte Rendue à l'Académie des Sciences IIb* 328, 5–10.
- Robisson, A., 2000. Comportement visco-hyperlastique endommageable d'élastomères SBR et PU: Prévision de la dureté de vie en fatigue, PhD thesis, Ecole Nationale Supérieure de Paris, France.
- Treloar, L.R.G., 1954. The photoelastic properties of short-chain molecular networks. *Transactions of the Faraday Society* 50, 881–896.
- Treloar, L.R.G., 1975. *The Physics of Rubber of Elasticity*. Oxford University Press, New York.
- Treloar, L.R.G., Riding, G., 1979. A non-Gaussian theory for rubber in biaxial strain: I. Mechanical properties. *Proceeding of the Royal Society of London, Series A* 369, 261–280.
- Wang, M.C., Guth, E., 1952. Statistical theory of networks of non-gaussian flexible chains. *Journal of Chemical Physics* 20, 1144–1157.
- Wu, P.D., van der Giessen, E., 1993. On improved network models for rubber elasticity and their applications to orientation hardening in glassy polymers. *Journal of Mechanics and Solids* 41 (3), 427–456.